Tracer Diffusion of 3-Arm and 12-Arm Star Polystyrenes in Dilute, Semidilute, and Concentrated Poly(vinyl methyl ether) Solutions

T. P. Lodge,* P. Markland,† and L. M. Wheeler‡

Department of Chemistry, University of Minnesota, Minneapolis, Minnesota 55455.
Received October 12, 1988; Revised Manuscript Received February 1, 1989

ABSTRACT: Tracer diffusion coefficients, D, for two 3-arm star ($M_w = 3.79 \times 10^5$ and 1.19×10^6) and for four 12-arm star ($M_w = 5.5 \times 10^4$, 4.67×10^5, 1.11×10^6, and 1.69×10^6) polystyrenes (PS) have been measured in solutions of poly(vinyl methyl ether) (PVME)/*o*-fluorotoluene, by dynamic light scattering. PVME matrix concentrations ranged up to 0.30 g/mL, with molecular weights $P_w = 1.4 \times 10^5$, 6.3×10^5, and 1.3×10^6. The PS radii of gyration were also measured by static light scattering, for one linear ($M_w = 1.05 \times 10^6$), one 3-arm star ($M_w = 1.19 \times 10^6$), and one 12-arm star ($M_w = 1.69 \times 10^6$) PS in PVME ($P_w = 2.5 \times 10^5$) solutions, over the concentration range $0 \le c \le 0.05$ g/mL. The mobility of the stars has been compared to that for the linear polymers reported in the preceding article, under identical solution conditions. The ratio D_{star}/D_{linear} for a given set of solution conditions was computed in two ways, either at constant arm molecular weight (i.e., viewing a linear molecule as a 2-arm star) or at constant total molecular weight. In the former case, above concentrations that scale approximately as c_e, the entanglement concentration for the PVME, the ratio D_{star}/D_{linear} decreases substantially with increasing concentration, for both 3-arm and 12-arm stars. This observation indicates that in entangled solutions, the mechanism(s) for diffusion depends on diffusant architecture. At constant total molecular weight, for 12-arm stars, the ratio D_{star}/D_{linear} increases slightly with increasing concentration, due to the earlier onset of entanglement effects for the spatially larger linear molecules. The measured PS radii of gyration decrease with increasing matrix concentration in a manner that is independent of PS architecture. These data were directly comparable to those reported for PS in PS/toluene by small-angle neutron scattering, indicating that in this ternary system the small, negative PS–PVME interaction parameter has little effect on macroscopic chain properties.

Introduction

As discussed in the preceding paper, henceforth referred to as part 1,[1] there remain unresolved, fundamental issues in understanding the dynamics of polymer molecules in semidilute and concentrated solutions. On the one hand, advances in experimental technique, computer simulation, and theory have all increased the general understanding of polymer solution dynamics. In particular, measurements of translational diffusion have been shown to provide a molecular-level picture of mechanisms of motion in polymer systems. Nevertheless, despite a growing body of data for linear polymers, it has still not proven possible to establish the relative importance of hydrodynamic interactions and topological constraints in determining molecular mobility and relaxation in solution. The diffusion of model branched polymers, however, provides a unique opportunity to gain further insight into the mechanisms of motion, for both linear and branched molecules. Furthermore, such experimental information can also have immediate technological significance. For example, the characterization of long-chain branching remains a recalcitrant problem. Branching occurs readily in both natural and synthetic polymers, producing widely differing architectures in terms of the number, length, and distribution of branches. Since these variations in topology may occur by design or as an unwanted side reaction, it is important to know their role in molecular and macroscopic properties such as diffusion and viscosity. The increasing availability of model polymers with controlled architecture permits a more quantitative investigation of the effects of chain branching and comparison to predictions based on various postulated mechanisms of motion.

In part 1, physical pictures for the diffusion of linear polymers in concentrated solution were classified into four groups. These were the basic reptation-plus-scaling approach,[2,3] the modified reptation theories such as those of Hess[4,5] and Kavassalis and Noolandi,[6-8] various constrained dynamics treatments,[9-11] and the Phillies hydrodynamic interaction model.[12-14] It was shown that the predictions of the reptation-plus-scaling approach, namely, $D \sim N^{-2}P^0c^{-1.75}$, where M and P are the molecular weights of the diffusant and matrix, respectively, and c is the matrix concentration, have never been observed simultaneously for one polymer/solvent system; regimes where each of these scaling laws is apparently obeyed individually have been reported. Further, it was argued that even though there have been several studies of linear polymer diffusion in semidilute and concentrated solutions, it has not really proved possible to eliminate any of these four classes of models on the basis of diffusion data alone. However, the consideration of branched polymer diffusion does present a potentially critical test. Simply stated, in the reptation picture, branched polymers should diffuse considerably less rapidly than linear molecules of comparable size,[15] while (as yet) neither the constrained dynamics models nor the Phillies picture make any distinction based on the architecture of the diffusing chain.

It is well-established that in very dilute solution the mechanism of diffusion for star-branched and linear polymers is essentially identical; both molecules may be viewed as equivalent spheres with a hydrodynamic radius that scales with M^ν, with $0.5 \le \nu \le 0.6$. Thus, although the prefactors depend on the detailed chain architecture, in both cases $D \sim M^{-\nu}$. In the melt, there have recently been a series of studies of 3-arm star diffusion. These include the infrared–microdensitometry measurements of Klein et al.,[16,17] the small-angle neutron scattering results of Bartels et al.,[18] the forced Rayleigh scattering experiments of Antonietti and Sillescu,[19] and the forward recoil spectrometry measurements of Shull et al.[20] In all cases, the results were consistent with the reptation picture, not only in that $D_{linear} \gg D_{star}$ but also in that $D_{star} \sim \exp\{kM_a\}$, where M_a is the arm molecular weight. On the basis of these results, a transition from hydrodynamically dominated diffusion in dilute solution to topologically con-

* Author to whom correspondence should be addressed.
† Current address: Upjohn Co., Kalamazoo, MI 49001.
‡ Current address: Exxon Chemical Americas, Linden Technology Center, Linden, NJ 07036.

0024-9297/89/2222-3409$01.50/0

strained diffusion in the melt should be observed as a function of increasing concentration.

In the first reported investigation of this transition region, for trace quantities of 3-arm star polystyrenes in a high molecular weight, linear poly(vinyl methyl ether) (PVME) matrix, the conditions necessary for the crossover between the two types of behavior were examined.[21] The diffusion coefficients for the 3-arm stars were compared to the values for equivalent linear polymers as a function of matrix polymer concentration from infinite dilution to 0.10 g/mL. As expected, in dilute solution, differences in the relative diffusion coefficients for the linear and star-branched probes could be attributed to differences in the hydrodynamic radii, but at higher concentrations, the ratio D_{star}/D_{linear} decreased substantially. These data were consistent with the idea that once both probe and matrix were sufficiently entangled, the linear probes were significantly more mobile than the stars. In this paper, we report more extensive measurements of D, for both 3-arm and 12-arm stars, in three different molecular weight PVME matrices. The matrix concentration range examined, up to at least 0.10 g/mL and up to 0.30 g/mL in some cases, extends through the semidilute and into the concentrated regime. Furthermore, concentrations at which the viscoelastic properties could be expected to show the effects of interchain entanglement have been exceeded. The results are discussed in terms of the effect of diffusant architecture on chain mobility and then with reference to the various models identified above.

In addition to the dynamic light scattering measurements of star diffusion, static light scattering has been used to measure the change in tracer polystyrene coil dimensions with increasing matrix concentration, for one 3-arm star, one 12-arm star, and one linear molecule. These results confirm the inference reported previously[22,23] that the tracer chains contract noticeably with increasing matrix concentration, and in a way which suggests that the influence of the slightly negative polystyrene–poly(vinyl methyl ether) interaction parameter is negligible. It is also demonstrated that the onset of coil contraction can occur in solutions for which the matrix component is still dilute.

Experimental Section

Samples and Solutions. The synthesis and characterization of the polystyrene (PS) samples have been described previously.[24] Two 3-arm and four 12-arm star PS were used: 3-arm stars PSJ-3A ($M_w = 1.19 \times 10^6$) and PSG-3A ($M_w = 3.79 \times 10^5$) and 12-arm stars PS-10-12 ($M_w = 1.69 \times 10^6$), PS-7-12 ($M_w = 1.11 \times 10^6$), PS-4-12 ($M_w = 4.67 \times 10^5$), and PS-9-12 ($M_w = 5.5 \times 10^4$). The polydispersities are all less than 1.1. The poly(vinyl methyl ether) (PVME) samples were the same as described in part 1, with $M_w = 1.3 \times 10^6$, 6.3×10^5, and 1.4×10^5 and polydispersities of approximately 1.6. A further, unfractionated PVME sample with $M_w \approx 2.5 \times 10^5$ was used in the static light scattering (SLS) measurements. The *o*-fluorotoluene (oFt) solvent (Aldrich Chemical Co.) was filtered three times with 0.05-μm Millipore filters and, for SLS, also distilled prior to use. Details of the solution preparation protocol were described briefly in part 1 and more extensively elsewhere.[22,25] The PS concentrations were maintained at approximately 0.1 c^*_{PS}, where c^*_{PS}, the coil overlap concentration for the PS, was estimated from SLS data of star-branched PS in toluene.[26] At these small but finite probe concentrations, there is less than a 5% difference between the measured, mutual diffusion coefficient, D, and the tracer diffusion coefficient of the PS component, in this ternary system.[23] Therefore, the reported D values are not corrected to $c_{PS} = 0$. Because of the dilution scheme, there was some fluctuation in c_{PS} for a given cell as a function of the PVME concentration, c. Table I lists the mean value and range of c_{PS} for each cell. All dynamic light scattering (DLS) measurements were made at 30.0 ± 0.1 °C.

Sample preparation for the SLS measurements followed a similar procedure, except that each solution was refiltered immediately before it was introduced into the instrument. Four solutions with c_{PS} ranging from $0.015c^*_{PS}$ to $0.5c^*_{PS}$ were prepared in oFT and also in ternary solutions with $c = 0.05$ g/mL. Further ternary solutions were prepared either by diluting the $c = 0.05$ g/mL solutions or by adding PVME/oFT stock solution to the PS/oFT series, again holding c_{PS} approximately constant. SLS data were collected at room temperature (26 ± 2 °C).

Table I
Mean and Range of PS Concentrations for Each Dilution Series

M	c, mg/mL		
	$P = 1.3 \times 10^6$	$P = 6.3 \times 10^5$	$P = 1.4 \times 10^5$
	3-Arm Star PS		
1.19×10^6	0.50 ± 0.03	0.54 ± 0.04	0.51 ± 0.02
3.79×10^5	0.72 ± 0.03	0.72 ± 0.02	0.74 ± 0.03
	12-Arm Star PS		
1.69×10^6	0.62 ± 0.03		0.63 ± 0.02
1.11×10^6	1.03 ± 0.08		1.06 ± 0.04
4.67×10^5	2.64 ± 0.03		2.62 ± 0.04
5.5×10^4	10.5 ± 0.1		10.6 ± 0.5

Measurements. DLS data were collected on a home-built DLS spectrometer and a 136-channel multisample time correlator (Brookhaven Instruments BI-2030). Details of the apparatus and data analysis were described briefly in part 1 and more extensively elsewhere.[22,25,27] A Wyatt Dawn-F SLS Instrument was used to measure the probe radius of gyration, R_g, and second virial coefficient, A_2, as a function of matrix concentration from 0.0 to 0.05 g/mL. The apparatus has a flow-through capillary cell for use as a size-exclusion chromatography detector, which requires a very small sample volume (≈0.1 mL) but manages to avoid reflections at the solvent/glass interface. However, it can also be used in a "batch" mode, i.e., with no imposed flow, as for the measurements reported here. Data were collected simultaneously at up to 15 detectors (4 photomultiplier tubes and 11 photodiodes) positioned around the scattering cell, with the scattering angles fixed but depending on the refractive index of the solvent. Values of R_g and A_2 for a linear ($M_w = 1.05 \times 10^6$), 3-arm ($M_w = 1.19 \times 10^6$), and 12-arm ($M_w = 1.69 \times 10^6$) star were obtained from Zimm plots for each PVME concentration. The general procedures for normalization, calibration, and data collection were as follows. Dark current offsets for each detector were determined with the laser turned off. Individual detector responses were normalized to the value of the photomultiplier at a scattering angle of 90° for a solution of a small isotropic scatterer (PS, with $M_w = 9 \times 10^3$). The "solvent" scattering was then measured with the appropriate PVME/oFT solution, and finally, the Rayleigh ratio was calibrated directly from the ternary solution data from the known molecular weight of the polystyrene. Since these measurements were made, the detectors in the SLS instrument have all been upgraded, with the result that all 15 of the detectors provide useful data, with reduced scatter relative to the data presented here. Nevertheless, the resulting values of R_g and A_2 have not changed.

Results and Discussion

The following section is divided into four parts. First, the diffusion data are presented and examined in terms of their dependence on matrix concentration. Second, the star mobility is compared to that of linear polymers in the same matrices, drawing heavily on the data presented in part 1. Third, the diffusion of the 3-arm stars is compared with that of the 12-arm stars. Finally, the dependence of the radius of gyration on matrix concentration for both star and linear tracers is discussed.

Concentration Dependence. The measured diffusion coefficients, D, of the two 3-arm and four 12-arm stars in three matrix molecular weights, P, are plotted versus c in Figures 1–3, in a log–log format. Figure 1 shows the concentration dependence of D for the 12-arm stars with $P = 1.3 \times 10^6$ and c ranging from 0.001 to 0.10 g/mL; the data are also listed in Table II. Since c varied slightly

Table II
Diffusion Coefficients for 12-Arm Star PS in PVME, $P = 1.3 \times 10^6$, Corrected for the Concentration Dependence of the Local Friction

	log $(D\zeta/\zeta_0)$, cm²/s			
log c, g/mL	$M = 1.69 \times 10^6$	$M = 1.11 \times 10^6$	$M = 4.67 \times 10^5$	$M = 5.5 \times 10^4$
-3.000	-6.94	-6.85	-6.63	-6.17
-2.854	-6.96	-6.86	-6.65	-6.22
-2.699	-7.00	-6.90	-6.68	-6.22
-2.523	-7.07	-6.96	-6.74	-6.25
-2.398	-7.13	-7.02	-6.79	-6.27
-2.222	-7.25	-7.14	-6.88	-6.30
-2.097	-7.36	-7.25	-6.96	-6.34
-2.000	-7.46	-7.33	-7.03	-6.36
-1.854	-7.64	-7.51	-7.15	-6.41
-1.699	-7.86	-7.70	-7.30	-6.47
-1.522	-8.20	-7.99	-7.53	-6.57
-1.398	-8.50	-8.24	-7.72	-6.65
-1.222	-8.88	-8.59	-7.92	-6.69
-1.097	-9.27	-8.96	-8.18	-6.78
-1.000	-9.65	-9.30	-8.43	-6.90

between replicate measurements on one solution, and also among the various PS solutions at a given nominal c, the data have been scaled to the exact concentrations listed in Tables II and III, using the function proposed by Phillies (see eq 1). The corresponding diffusion coefficients with $P = 1.4 \times 10^5$ have been reported previously.[25] In Figures 2 and 3, log D is plotted versus log c for three values of P, for the 1.19×10^6 and 3.79×10^5 3-arm stars, respectively; these data are also listed in Table III. Most of the data for $P = 1.3 \times 10^6$ have been presented previously.[21] The concentration range extends from 0.001 to 0.20 g/mL for the 3-arm stars with $P = 1.3 \times 10^6$ and 6.3×10^5 and from 0.001 to 0.30 g/mL when $P = 1.4 \times 10^5$.

In general, the values of D decrease smoothly with increasing c and M. Also, for constant M, the curvature of the data increases with P, indicating that the diffusion of the probe depends on the matrix chain mobility. Also plotted in these three figures, and listed in Tables IV and V, are the fits to the stretched exponential function suggested by Phillies[12-14]

$$D(c) = D_0 \exp\{-\alpha c^u\} \quad (1)$$

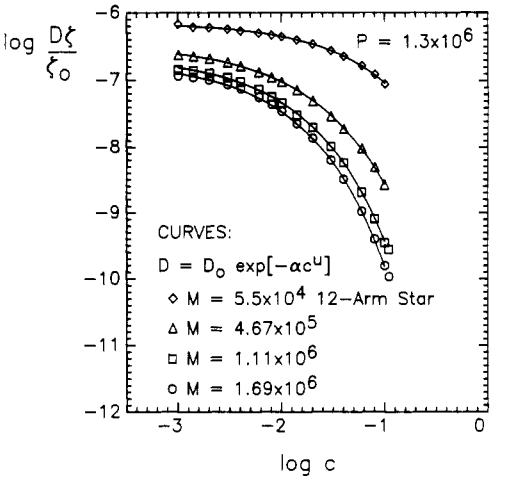

Figure 1. PS 12-arm star diffusivity, corrected for changing local friction, as a function of PVME concentration with $P = 1.3 \times 10^6$. The fitting function is indicated on the plot, with D_0 left as a floating parameter.

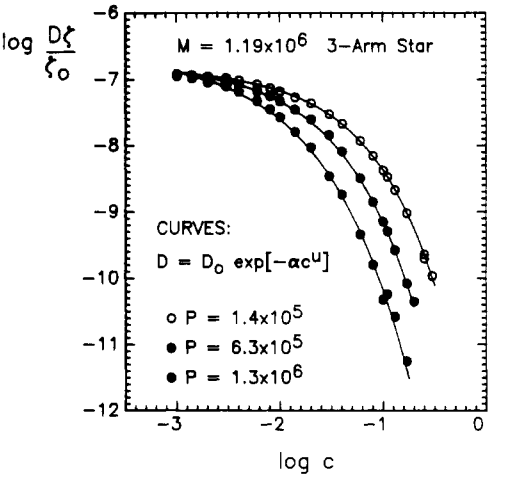

Figure 2. PS 3-arm star ($M = 1.19 \times 10^6$) diffusivity, corrected for changing local friction, as a function of PVME concentration with $P = 1.4 \times 10^5$, 6.3×10^5, and 1.3×10^6. The fitting function is indicated on the plot, with D_0 left as a floating parameter.

Table III
Diffusion Coefficients for 3-Arm Star PS in PVME, Corrected for the Concentration Dependence of the Local Friction

	log $(D\zeta/\zeta_0)$, cm²/s					
	$P = 1.4 \times 10^5$		$P = 6.3 \times 10^5$		$P = 1.3 \times 10^6$	
log c, g/mL	$M = 1.19 \times 10^6$	$M = 3.79 \times 10^5$	$M = 1.19 \times 10^6$	$M = 3.79 \times 10^5$	$M = 1.19 \times 10^6$	$M = 3.79 \times 10^5$
D_0	-6.92	-6.59				
-3.000	-6.92	-6.59	-6.93	-6.69	-6.95	-6.67
-2.854	-6.94	-6.67	-6.95	-6.70	-6.98	-6.66
-2.699	-6.96	-6.69	-6.97	-6.72	-7.04	-6.71
-2.523	-6.98	-6.72	-7.02	-6.75	-7.11	-6.78
-2.398	-7.02	-6.74	-7.08	-6.79	-7.19	-6.81
-2.222	-7.08	-6.80	-7.18	-6.86	-7.33	-6.90
-2.097	-7.13	-6.85	-7.26	-6.92	-7.46	-6.99
-2.000	-7.18	-6.89	-7.26	-6.92	-7.58	-7.09
-1.854	-7.27	-6.98	-7.33	-6.98	-7.80	-7.19
-1.699	-7.36	-7.05	-7.46	-7.09	-8.03	-7.54
-1.522	-7.53	-7.20	-7.86	-7.39	-8.50	-7.70
-1.398	-7.67	-7.33	-8.09	-7.56	-8.75	-7.77
-1.222	-7.93	-7.56	-8.50	-7.86	-9.34	-8.13
-1.097	-8.17	-7.78	-8.86	-8.13	-9.80	-8.42
-1.000	-8.38	-7.98	-9.15	-8.39	-10.32	-8.71
-0.959	-8.48	-8.07	-9.30	-8.54	-10.24	-8.85
-0.886	-8.68	-8.25	-9.58	-8.73	-10.58	-9.13
-0.770	-9.02	-8.57	-10.08	-9.18	-11.25	-9.62
-0.699	-9.26	-8.80	-10.35	-9.46		-10.03
-0.602	-9.64	-9.19				
-0.523	-9.97	-9.49				

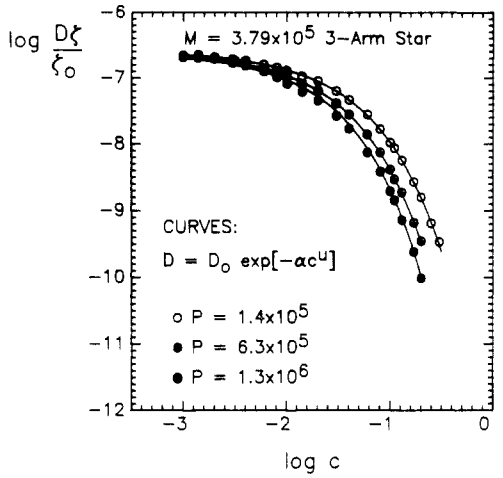

Figure 3. PS 3-arm star ($M = 3.79 \times 10^5$) diffusivity, corrected for changing local friction, as a function of PVME concentration with $P = 1.4 \times 10^5$, 6.3×10^5, and 1.3×10^6. The fitting function is indicated on the plot, with D_0 left as a floating parameter.

Table IV
Phillies Parameters for 12-Arm Star PS Using Floated and Fixed D_0[a]

P	M	$10^7 D_0$	α, g/mL	α, mg/mL	u
		Floated D_0			
1.4×10^5	1.69×10^6	1.56	18.0	0.186	0.662
	1.11×10^6	1.91	17.5	0.187	0.657
	4.67×10^5	2.98	16.3	0.164	0.666
	5.50×10^4	7.72	11.9	0.0638	0.757
1.3×10^6	1.69×10^6	1.87	29.3	0.413	0.617
	1.11×10^6	2.24	26.0	0.390	0.608
	4.67×10^5	3.38	18.3	0.338	0.578
	5.50×10^4	7.10	8.87	0.111	0.634
		Fixed D_0			
1.4×10^5	1.69×10^6	1.10	19.5	0.112	0.747
	1.11×10^6	1.42	18.7	0.120	0.731
	4.67×10^5	2.52	17.1	0.122	0.716
	5.50×10^4	7.33	11.8	0.0598	0.765
1.3×10^6	1.69×10^6	1.10	35.9	0.224	0.735
	1.11×10^6	1.42	31.8	0.217	0.722
	4.67×10^5	2.52	21.8	0.207	0.674
	5.50×10^4	7.33	8.44	0.127	0.608

[a] Fit to data corrected for $\zeta(c)$.

with α, u, and D_0 left as free parameters. The interpretation of these fits and resulting parameter values were discussed in part 1; it can be seen that eq 1 describes the concentration dependence of D extremely well in all cases. Certainly, the model proposed to account for the clear success of eq 1 in fitting diffusion data takes no account of diffusant architecture and therefore cannot explain the results to be displayed in Figures 7–10. Having fit the data successfully with eq 1, one can note that in general the values for u are slightly larger for stars than for linear polymers, but there is nothing in the model that would predict this behavior. The success of eq 1 in fitting the data is extremely useful, however, if for no other purpose than the interpolation of the data to particular concentrations, as mentioned above.

The data in Figures 1–3 have been corrected for the concentration dependence of the local friction, $\zeta(c)$, from the concentration dependence of the solvent diffusion, as described in part 1. However, as pointed out in part 1, the change in local friction as estimated in this way is relatively small, D_{0FT} falling by a factor of 0.38 by $c = 0.30$ g/mL. Furthermore, since there are as yet no specific model predictions for the c dependence of D for stars, except for eq 1, the correction for changing local friction is of less importance. In order to divide the data into concentration

Table V
Phillies Parameters for 3-Arm Star PS Using Floated and Fixed D_0[a]

P	M	$10^7 D_0$	α, g/mL	α, mg/mL	u
		Floated D_0			
1.3×10^6	1.19×10^6	2.50	29.2	0.657	0.549
	3.79×10^5	2.36	23.8	0.188	0.701
6.3×10^5	1.19×10^6	1.82	22.6	0.340	0.607
	3.79×10^5	2.51	19.8	0.179	0.681
1.4×10^5	1.19×10^6	1.47	16.0	0.174	0.653
	3.79×10^5	2.53	15.2	0.139	0.679
		Fixed D_0			
1.3×10^6	1.19×10^6	1.19	35.6	0.350	0.669
	3.79×10^5	2.24	24.2	0.175	0.714
6.3×10^5	1.19×10^6	1.19	24.8	0.216	0.687
	3.79×10^5	2.24	20.6	0.149	0.714
1.4×10^5	1.19×10^6	1.19	16.6	0.132	0.700
	3.79×10^5	2.24	15.5	0.116	0.709

[a] Fit to data corrected for $\zeta(c)$.

Table VI
Estimated Values of c^* and c_e

M	c^*, g/mL	c_e, g/mL
	3-Arm Star PS	
1.19×10^6	0.0071	0.023
3.79×10^5	0.016	0.071
	12-Arm Star PS	
1.69×10^6	0.030	0.078
1.11×10^6	0.041	0.096
4.67×10^5	0.090	0.234
5.5×10^4	0.39	
	Linear PS	
1.05×10^6	0.0042	0.018
4.22×10^5	0.0085	0.042
1.79×10^5	0.017	0.10
6.5×10^4	0.037	0.27
	Linear PVME	
1.3×10^6	0.0033	0.006
6.3×10^5	0.0057	0.012
1.4×10^5	0.011	0.05

regimes, estimates of the crossover concentrations, c^* and c_e, for PS and PVME are obtained as follows. The definition of c^* for the matrix polymer is taken to be $1.5/[\eta]$, while for PS it is taken to be $3M/(4\pi N_a R_g^3)$ (these definitions are essentially equivalent via the Flory–Fox relation). As in part 1, the critical concentrations for entanglement, c_e, have been estimated as $\rho M_e^0/M$, where ρ is the polymer density and M_e^0 is the molecular weight between entanglements for the bulk polymer (7200 for PVME and 18000 for PS). The values of c^* and c_e are listed in Table VI.

It was shown in part 1 that D/D_0, corrected for $\zeta(c)$, could be scaled together to form one master curve versus c for all M and P, using an empirical shift factor, c'. Furthermore, it was demonstrated that c' could be well-represented as $(c^*_{PS}c^*_{PVME})^{0.5}$. In Figure 4, the same approach has been attempted for both the 3-arm and the 12-arm stars, in all three matrices. Again, it can be seen that a master curve can be obtained. At lower values of c the superposition is not quite so good, primarily because D/D_0 approaches one as c approaches zero at different rates for the 3-arm and 12-arm stars. In Figure 5, the resulting values of c' are normalized to c^*_{PS} and plotted logarithmically against $2N_{a,M}/N_P$, where N is the degree of polymerization and $N_{a,M}$ is the arm degree of polymerization. Thus, $2N_{a,M}$ is the so-called span molecular weight and represents a measure of the spatial extent of the star for any functionality f. Also included in this plot are the values of c' obtained for the linear PS, as shown

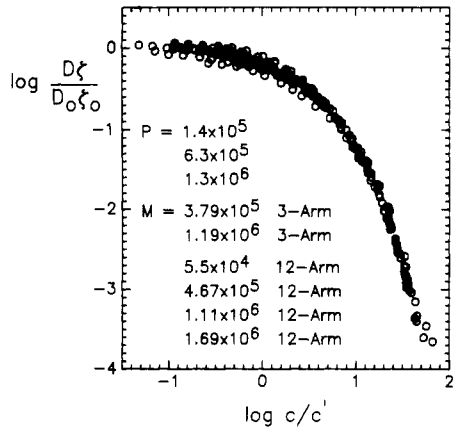

Figure 4. Normalized PS 3-arm star and 12-arm star diffusivity, corrected for changing local friction, as a function of reduced PVME concentration, for $P = 1.4 \times 10^5$, 6.3×10^5, and 1.3×10^6.

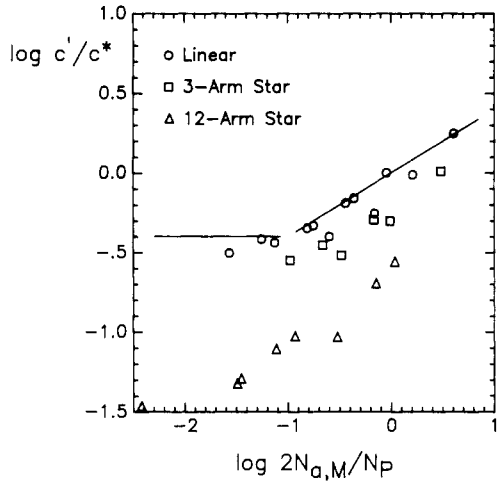

Figure 5. Reference concentration, c', normalized to c^* for each PS, as a function of the ratio of the span degree of polymerization to PVME degree of polymerization, for linear, 3-arm star, and 12-arm star PS. The illustrative straight lines are retained from Figure 13 of part 1.

in Figure 13 in part 1, and the accompanying illustrative straight lines. Some additional explanation of Figure 5 is appropriate. For all three cases, linear, 3-arm, and 12-arm polymers, the data were displaced along the log c axis until the best superposition was obtained with the actual data for the 1.05×10^6 linear tracer in the $P = 1.3 \times 10^6$ matrix. Then, c' was normalized to c^* calculated for the tracer in question. For the stars, the values of c^* were estimated by the formula identified above, using the measured R_g values of Khasat et al.[26] Finally, the values of c' were scaled simply to make $c' = c^*$ when $N_M = N_P$ for the linear PS. The degree of polymerization is used here instead of molecular weight to account (approximately) for the differences in monomer molecular weight and also entanglement length, as discussed in part 1.

There are two important conclusions to be drawn from Figures 4 and 5. First, the relative values of c' required to achieve superposition are strong functions of f. In particular, for a given ratio of tracer span length to matrix polymer length, the more arms the star has, the larger the shift factor necessary to bring the data in line with the chosen reference linear polymer. This is a direct reflection of the fact that the star diffusion begins to decrease with increasing c more rapidly than does the linear diffusion. This point will be examined in more detail in the next section. The second conclusion is that log $(D\zeta/D_0\zeta_0)$ can be superposed by a horizontal shift, for linear and star

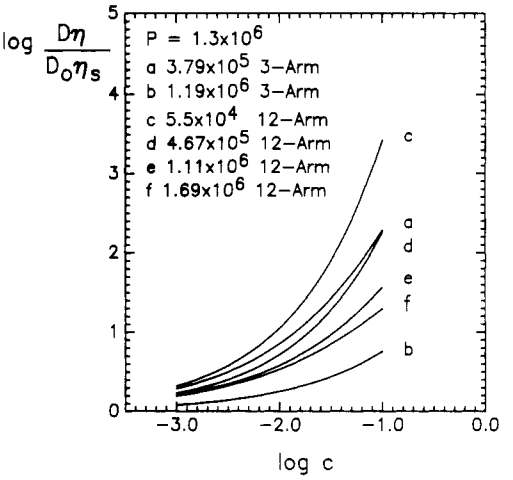

Figure 6. Normalized product of PS diffusivity and PVME solution viscosity, as a function of PVME concentration, for $P = 1.3 \times 10^6$. The actual data are represented by smooth curves for clarity.

polymers. This implies some universality to the functional form involved. The success of the superposition, in fact, requires that the values of u in eq 1 not vary much over the range of solutions examined. Indeed, the values generally fall between 0.6 and 0.7 throughout, with no strong suggestion of approaching either of the predicted limits (0.5 when $P \to \infty$ and 1 when $P \to 0$).[12-14] It also suggests that the functional form describing D for linear and star polymers cannot be too different. At the same time, as pointed out in part 1 and as emphasized throughout this paper, the data are almost all in a transition region where the tracer and matrix polymers are either almost, or only just, entangled, and furthermore the transition from dilute solution toward limiting concentrated solution or melt behavior is a very gradual one. Thus, the universality implied by Figure 4 applies more to the transition than to the low or high c limiting behavior.

In Figure 6, the product $D\eta/D_0\eta_s$ is plotted logarithmically against c, for the stars in $P = 1.3 \times 10^6$ solutions. The viscosity data were presented in part 1. For the sake of clarity, the actual data have been replaced in Figure 6 by smooth curves obtained from fitting D and η to eq 1 and to its analogue, respectively. Just as in part 1, this format can be used to reveal the rather limited extent of "Stokes-Einstein" diffusion, i.e., where the tracer can be viewed as an equivalent hydrodynamic sphere diffusing in a viscous medium. As with the linear data, this product always rises with increasing c, indicating that even for star polymers diffusivity is reduced by a smaller factor than viscosity is increased. The effect is reduced for larger stars, however, suggesting that in the limit of large M and/or large f, a much broader Stokes-Einstein regime might be observed.

Star versus Linear Tracer Diffusion. The influence of molecular architecture on probe mobility can be evaluated by comparing the diffusion of linear and star-branched polymers. Since linear molecules can be viewed as 2-arm stars, this comparison can be made for probes with equal arm molecular weight, M_a, as shown in Figures 7–10. The relative diffusivities are expressed as $[D_B/D_{0,B}]/[D_L/D_{0,L}]$, where the rationale for this approach is 2-fold. First, since the ratios are calculated at fixed c, $\zeta(c)$ is factored out. Second, the normalization of D_B/D_L with respect to the probe D_0 values accounts for the differences in mobility at infinite dilution, where intramolecular hydrodynamic interaction dominates the diffusion mechanism. Therefore, it is expected that $[D_B/D_{0,B}]/[D_L/D_{0,L}]$

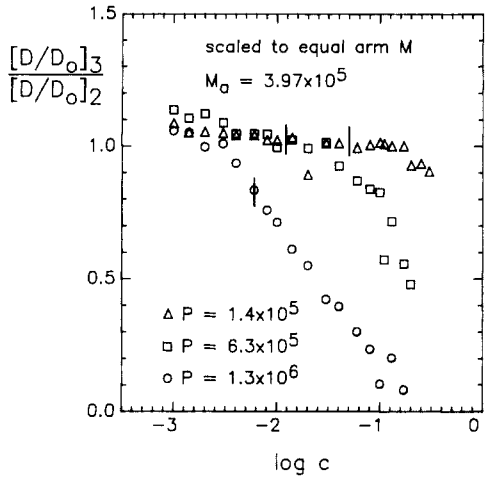

Figure 7. Normalized ratio of PS 3-arm star to PS linear diffusivity, at constant $M_a = 3.97 \times 10^5$, as a function of PVME concentration, for $P = 1.4 \times 10^5$, 6.3×10^5, and 1.3×10^6. The vertical lines denote c_e for the matrices.

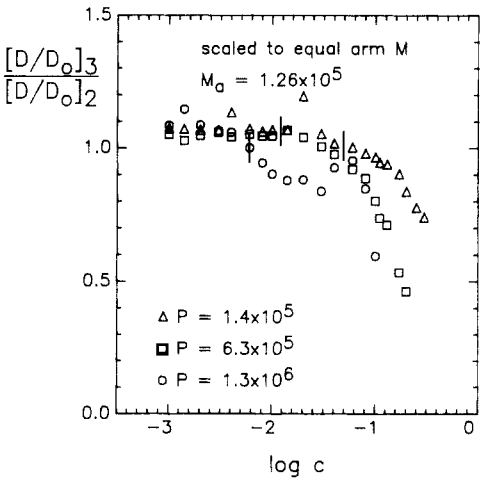

Figure 8. Normalized ratio of PS 3-arm star to PS linear diffusivity, at constant $M_a = 1.26 \times 10^5$, as a function of PVME concentration, for $P = 1.4 \times 10^5$, 6.3×10^5, and 1.3×10^6. The vertical lines denote c_e for the matrices.

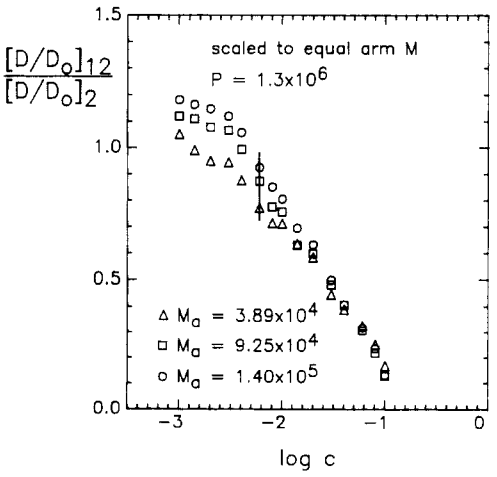

Figure 9. Normalized ratio of PS 12-arm star to PS linear diffusivity, at constant M_a, as a function of PVME concentration, for $P = 1.3 \times 10^6$. The vertical line denotes c_e for the matrix.

will be close to unity when the diffusion of both linear and star probes is governed by the hydrodynamic radius, whereas the ratio will deviate from unity when architecture-dependent diffusion mechanisms become significant. In Figure 7, values of $[D_B/D_{0,B}]/[D_L/D_{0,L}]$ are plotted

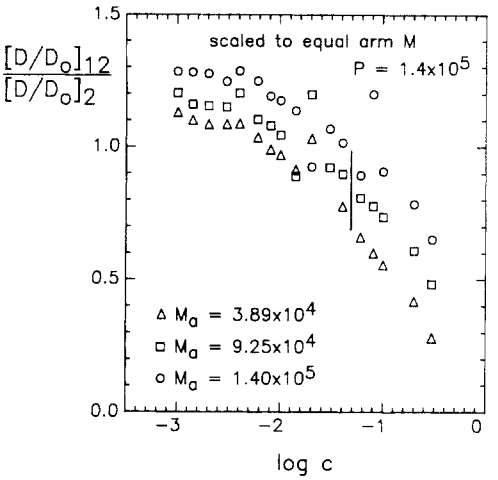

Figure 10. Normalized ratio of PS 12-arm star to PS linear diffusivity, at constant M_a, as a function of PVME concentration, for $P = 1.4 \times 10^5$. The vertical line denotes c_e for the matrix.

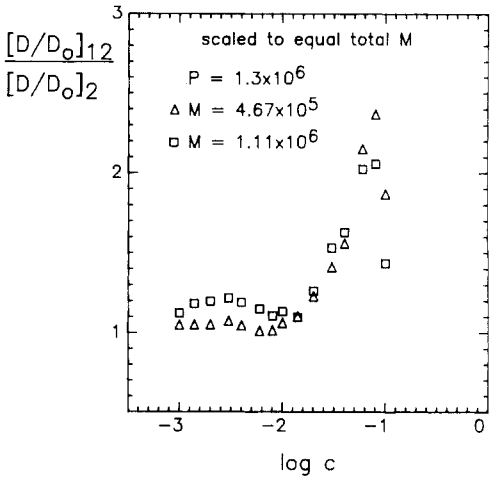

Figure 11. Normalized ratio of PS 12-arm star to PS linear diffusivity, at constant total M, as a function of PVME concentration, for $P = 1.3 \times 10^6$.

versus log c for the 1.19×10^6 3-arm star in the three PVME matrices. Figure 8 shows the same quantity for the 3.79×10^5 3-arm star in the same matrix solutions. In Figures 9 and 10, $[D_B/D_{0,B}]/[D_L/D_{0,L}]$ versus log c is plotted for the three largest 12-arm stars in the 1.3×10^6 and 1.4×10^5 PVME matrices, respectively. For the 5.5×10^4 12-arm star, the corresponding M_a is so small that D_L cannot be accurately extrapolated from the experimentally measured D_Ls, which have been obtained for PS with total M ranging from 6.5×10^4 to 1.05×10^6, and thus this 12-arm star is omitted from this plot. In all cases, the ratio $[D_B/D_{0,B}]/[D_L/D_{0,L}]$ decreases with increasing c, falling by as much as an order of magnitude over the concentration range examined. The onset of a significant decrease occurs at lower c for higher P.

The relative diffusion of linear and star-branched probes can also be compared at equal total molecular weight, fM_a, where f is the number of arms, as shown in Figures 11 and 12 for the two intermediate 12-arm stars; the largest and smallest 12-arm stars have total molecular weights that are outside of the corresponding range for the linear PS. For the 3-arm stars, the results of this calculation would be very similar to those in Figures 7 and 8, due to the small number of arms, and so these plots are not shown. However, for the 12-arm stars, the plots are different from Figures 9 and 10; the values of $[D_B/D_{0,B}]/[D_L/D_{0,L}]$ instead begin to increase slightly with increasing c.

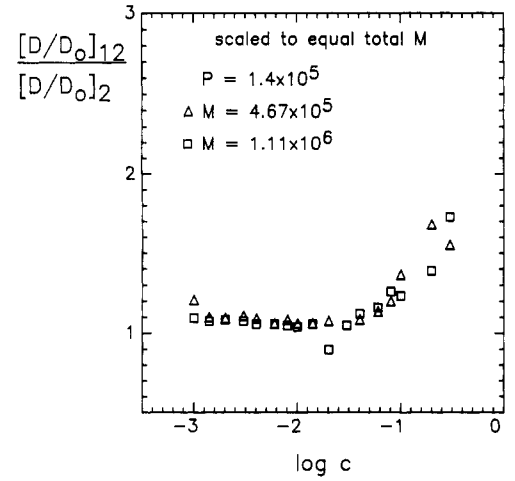

Figure 12. Normalized ratio of PS 12-arm star to PS linear diffusivity, at constant total M, as a function of PVME concentration, for $P = 1.4 \times 10^5$.

All values of the ratio $[D_B/D_{0,B}]/[D_L/D_{0,L}]$ were determined in a multistep process, involving first a calculation of D_B/D_L at each c, followed by normalization to the relative values at infinite dilution. The general procedure was as follows. The concentration dependence of four linear PS samples in all three matrices was reported in part 1. However, since the stars and linear polymers are not matched identically in either M or M_a, D_L values were interpolated in an appropriate manner. This determination was most straightforward for the linear PS when $P = 1.3 \times 10^6$, where D_L followed a power law with M, and D_L is calculated from the least-squares fit of the log D_L versus log M at each c. In the lower P solutions, however, there was slightly more uncertainty in the interpolations because of the curvature in the log D_L versus log M plots for a given c, as shown for example in Figures 6 and 7 in part 1. For these calculations, smooth curves were drawn through the data, and D_L was read directly off the plot. As indicated earlier, the range in M for the star-branched probes was not always within the range of the linear data. Since extrapolations to extreme molecular weights are uncertain, the set of comparisons for the 12-arm stars is not complete. (Previously reported D_B/D_L ratios for 12-arm stars with $P = 1.4 \times 10^5$ were calculated with linear data scaled from the D values with $P = 1.3 \times 10^6$.[25] These ratios have been recalculated here with the more recently obtained data for linear PS in this P, which accounts for the slight differences in the newly published values.) The resulting values of D_B/D_L were then normalized to measured values of $D_{0,B}$ and interpolated values of $D_{0,L}$. Although fairly successful for the 3-arm stars, this normalization leads to a systematic deviation from unity at low c for the 12-arm stars, which increases with star M_a. One reason for this is that as c decreases and M_a increases, D/D_0 converges to unity slightly more rapidly for the 12-arm stars than does the ratio for the linear or 3-arm star probes. As a result, the final ratio $[D_B/D_{0,B}]/[D_L/D_{0,L}]$ can actually exceed unity at small c. This also accounts to some extent for the lack of complete superposition in the low-c region in Figure 4, as discussed previously.

From Figures 7–10, it is apparent that the diffusion of star-branched polymers is hindered relative to linear PS of equal arm molecular weight and that this difference becomes more significant as either c or P is increased. In Figure 7, for the 1.19×10^6 3-arm star, $[D_B/D_{0,B}]/[D_L/D_{0,L}]$ begins to decrease significantly above a critical concentration which scales approximately as c_e for the matrix, indicated on the plot by short vertical lines. For the largest P, the decrease begins at a concentration just below c_e, but it should be emphasized that in the absence of extensive viscoelastic measurements on this system, the estimates of c_e are approximate. At $c = 0.20$ g/mL, the diffusivity of the star probe is $\approx 0.1 D_L$ for $P = 1.3 \times 10^6$, $\approx 0.5 D_L$ for $P = 6.3 \times 10^5$, and $\approx 0.9 D_L$ for $P = 1.4 \times 10^5$, so the effects of matrix mobility are clearly significant. The same general trends are observed in Figure 8, for the diffusion of the 3.79×10^5 3-arm star PS, although the reduction in $[D_B/D_{0,B}]/[D_L/D_{0,L}]$ is in general less than for the larger star. In Figure 9, the onset of hindered diffusion for the 12-arm stars in $P = 1.3 \times 10^6$ also begins just below c_e, although a probe molecular weight dependence is not as evident in this comparison. Finally, in Figure 10, $[D_B/D_{0,B}]/[D_L/D_{0,L}]$ again decreases with c, although the decrease is quite gradual, and again begins at a concentration slightly below c_e.

In Figure 11, the 12-arm stars actually diffuse faster than the linear counterparts in the nondilute solution region, where the ratios of the D values increase to 2.0–2.5 at $c = 0.10$ g/mL for $P = 1.3 \times 10^6$. For the smallest P, $[D_B/D_{0,B}]/[D_L/D_{0,L}]$ also increases with c for the 12-arm stars, with the increase amounting to less than a factor of 2 by $c = 0.30$ g/mL, as shown in Figure 12. This increase in the ratio is reasonable, since D_L in the denominator is much smaller than in the equal arm molecular weight comparison. In other words, a linear probe becomes entangled with the matrix at a lower matrix concentration than does a 12-arm star of equal total molecular weight. This is quite consistent with the viscosity–molecular weight relationship for melts of linear and star polymers. Thus, it is expected that the ratios for the 12-arm stars will also begin to decrease at concentrations higher than were measured, when the stars become significantly entangled; the highest concentration data points in Figure 11 may hint at this behavior.

The observation that star polymers diffuse more slowly than linear polymers of comparable size, once the solutions have become entangled, represents strong and direct evidence that the architecture of the diffusing chain has a significant influence on its mobility. As emphasized in part 1 and in the Introduction, to date only the reptation model is even qualitatively in agreement with this result. Furthermore, in agreement with the situation for linear polymer diffusion, where $c > c_e$ is a necessary condition for the onset of reptation-like behavior, the onset of architecture-dependent diffusion appears to require entanglement in the viscoelastic sense, and not merely coil overlap. The existence of a transition from hydrodynamically controlled to topologically controlled diffusion, previously inferred from measurements in dilute solution and in melts, now has direct confirmation.

The reptation model has been adapted to the case of branched polymers in a number of ways, beginning with the calculation of the arm retraction time by de Gennes.[15] These various approaches all arrive at the following functional form:

$$D_B(M) \sim M_a^{-x} \exp\{-kM_a(f-2)\} \qquad (2)$$

where f is the number of arms, k is a prefactor, and x adopts a value 1,[28] 2,[18,29] or 3.[15] Several points about eq 2 deserve emphasis. First, the calculations which lead to this form all assume that the matrix is effectively fixed on the time scale of arm relaxation. In solution, it will clearly be much harder than in the melt to satisfy this condition exactly. In fact, it is clear from Figures 1–3 that matrix mobility is playing a substantial role in D for the tracers. Second, the exponential dependence arises from the probability of an arm retracing its path toward the central

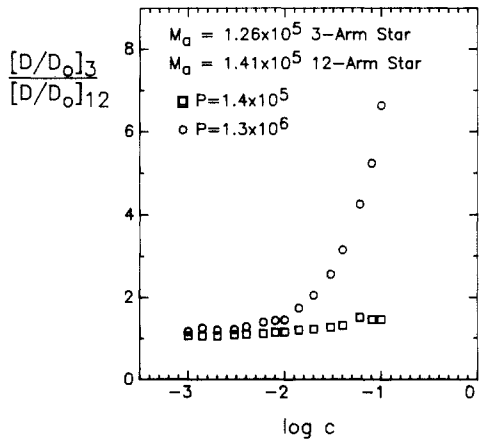

Figure 13. Normalized ratio of PS 3-arm star to PS 12-arm star diffusivity, at constant $M_a \approx 1.3 \times 10^5$, as a function of PVME concentration, for $P = 1.4 \times 10^5$ and 1.3×10^6.

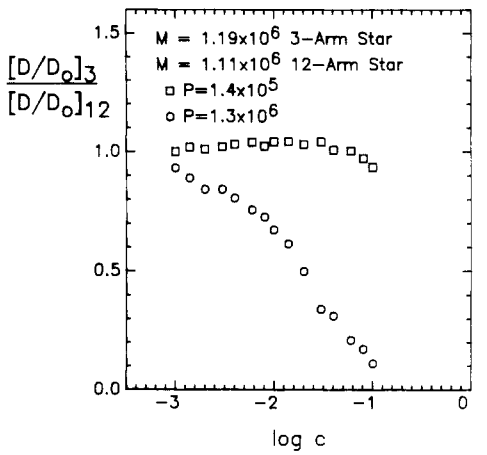

Figure 14. Normalized ratio of PS 3-arm star to PS 12-arm star diffusivity, at constant total $M \approx 1.1 \times 10^6$, as a function of PVME concentration, for $P = 1.4 \times 10^5$ and 1.3×10^6.

junction of the star, to permit some form of modified reptation through the matrix of fixed obstacles. The studies of 3-arm star diffusion in the melt have been consistent with this exponential dependence. However, to the extent that the matrix is mobile, this functional form may not be appropriate at all. The reason for this stems from the fact that the effectiveness of an entanglement or constraint in reducing star mobility depends very much on its location along an arm; those near the star center will still require substantial arm retraction, while those near the free end of an arm can be relaxed quite readily. Thus, a simple addition of a matrix relaxation contribution to eq 2 may not be the appropriate way to account for the contribution of matrix mobility. Third, in this picture there is an important distinction between the viscoelastic properties and the diffusion of a many-armed star. For relaxation after an imposed strain, the many arms of a star can relax essentially independently, and thus the relaxation time of the entire molecule should still scale with $\exp\{-kM_a\}$. For the diffusion by the arm retraction plus reptative step mechanism, $(f-2)$ arms need to relax more or less coherently, which in the limit of complete coherence would lead to a diffusion relaxation time scaling with $\exp\{-kM_a(f-2)\}$. For 3-arm stars, the difference is clearly moot. Recently, some measurements of 4-arm and 8-arm star PS diffusion in a microgel have been reported.[20] Surprisingly, the diffusion coefficients were essentially independent of the number of arms, suggesting that incoherent arm retraction was sufficient for diffusion. Since the largest arms were only 6×10^4 in molecular weight, this conclusion should perhaps be regarded as tentative. (On the other hand, the treatment of Rubinstein predicts that the f dependence should appear only in the prefactor in eq 2.[31]) However, the main point here is that, given the substantial P dependence evident in D, the limited number of star samples, and the relatively small number of entanglements per star, there is no reason to expect to see the dependence on M_a predicted by eq 2.

3-Arm versus 12-Arm Star Mobility. An interesting way to examine the results reported here is to form the ratio $D_{f=3}/D_{f=12}$ as a function of matrix concentration. As with the comparison to linear polymers, this ratio can be calculated at equal arm molecular weight or at equal total molecular weight. The resulting plots are shown in Figures 13 and 14, respectively, for both $P = 1.3 \times 10^6$ and $P = 1.4 \times 10^5$. As expected, in the lower molecular weight matrix, the ratio is essentially unity at all concentrations examined, because the matrix relaxation time is relatively short. This is consistent with the results in Figures 7, 8, and 10, for the branch-to-linear comparison at the same lower P. In the larger P matrix, however, at approximately equal arm molecular weight, the 3-arm star is more mobile than the 12-arm star. This is intuitively very reasonable; the addition of extra arms of equal length should only serve to reduce mobility. It is possible to make a prediction for this ratio, using eq 2, but for the reasons outlined above, such a prediction should not really be expected to apply in this transition region.

Table VII
Radii of Gyration for PS in PVME, $P = 2.5 \times 10^5$

	R_g, nm		
c, g/mL	linear $M = 1.05 \times 10^6$	3-arm star $M = 1.19 \times 10^6$	12-arm star $M = 1.69 \times 10^6$
0.0	45	42	30
0.004	43	34	29
0.006	41	38	28
0.010	39	36	28
0.020	38		
0.030	38	34	26
0.050	35	33	24

The case of equal total molecular weight, represented in Figure 14, is more interesting. Here it is not immediately obvious a priori whether the ratio should be greater than or less than unity. In other words, is a third, relatively long arm or are ten additional shorter arms more effective in reducing the mobility of the star? In this instance, eq 2 may be used as a guide. After forming the ratio D_3/D_{12} for the two stars, the resulting prefactor always predicts that the ratio should be less than unity, while the exponential term predicts an increase in the ratio. In the limit of very long arms, the exponential should dominate; clearly, this is not seen in Figure 14. On the other hand, if indeed coherent arm retraction is not necessary, then the exponential term cancels, and the ratio should approach some limiting value less than unity with increasing c. However, for the reason emphasized above, namely, that the stars are not sufficiently entangled for eq 2 to describe their behavior completely, it is not possible to say whether or not Figure 14 supports the idea of incoherent arm retraction.

Radius of Gyration. Static light scattering measurements have been made on the $M = 1.05 \times 10^6$ linear, $M = 1.19 \times 10^6$ 3-arm star, and $M = 1.69 \times 10^6$ 12-arm star PS in solutions of PVME, with $P = 2.5 \times 10^5$. Representative Zimm plots are shown in Figures 15 and 16 for the linear tracer at $c = 0.04$ g/mL and for the 3-arm star tracer at $c = 0.03$ g/mL, respectively. The normalized PS radii of gyration, $R_g(c)/R_{g,0}$, are plotted as a function of

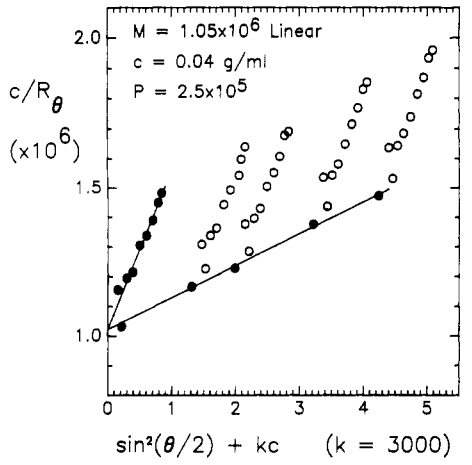

Figure 15. Zimm plot for linear PS, $M = 1.05 \times 10^6$, in PVME solutions with $P = 2.5 \times 10^5$ and $c = 0.04$ g/mL.

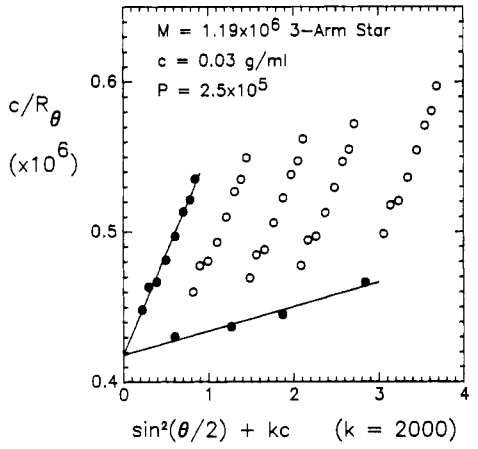

Figure 16. Zimm plot for 3-arm star PS, $M = 1.19 \times 10^6$, in PVME solutions with $P = 2.5 \times 10^5$ and $c = 0.03$ g/mL.

c/c^*_{PS} in Figure 17, and the measured values are listed in Table VII. This scaling of the concentration with c^*_{PS} is appropriate because the screening of the excluded volume is expected to occur when the overall concentration of the solution is equal to the monomer concentration inside the probe coil. Thus, to a first approximation, the onset of coil contraction for a probe chain should depend on M and c, but not P. Also, for the case $M > P$ considered here, $c^*_{PS} < c^*_{PVME}$, and thus the coil contraction begins when both $c_{PS} < c^*_{PS}$ and $c_{PVME} < c^*_{PVME}$. In other words, the solution is technically "dilute" for both components even though the excluded volume of the tracer chain begins to be screened. The issue of coil contraction in ternary solutions has been considered by Joanny et al.[32] for the case of $\chi_{12} = 0$ and by Nose for arbitrary χ_{12}.[33] These results presented here are in good agreement with these predictions. Neutron scattering measurements of $R_g(c)$ for linear PS ($M = 1.1 \times 10^5$) in binary solutions have been reported by Daoud et al.,[34] in CS_2, and more recently by King et al.,[35] in toluene. These data are included in Figure 17 and are very similar to those reported here, when plotted in this format.

The similarity between the binary and the ternary systems is a very interesting result and reflects the PS/PVME interaction parameter χ_{12}. For this pair, χ_{12} is very small and negative; a value of −0.01 has been reported.[36] As a result, even though PVME and PS are chemically distinct, the concentration dependence of the probe coil contraction is independent of P and only a function of c_{matrix}/c^*_{probe}. These results also strongly support the assumption that the behavior of dilute PS chains in PVME

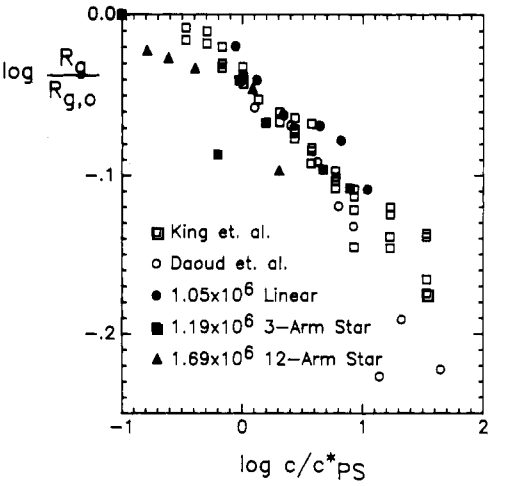

Figure 17. Normalized linear, 3-arm star, and 12-arm star PS radius of gyration as a function of PVME concentration normalized to c^* for the PS. Neutron scattering data for linear PS in PS solutions from ref 34 and 35 are included.

solutions is very similar to the behavior of PS chains in PS solutions. For the stars the concentration dependence of the coil contraction is similar to that of the linear probe, within experimental error; this is reasonable in that the contraction is governed by the thermodynamics, while the diffusion emphasizes frictional interactions. By $c = 0.05$ g/mL, the probe size has shrunk to 70–80% of its infinite dilution value but still is larger than its estimated Θ dimensions. Although these changes in coil dimensions are clearly measurable, they are relatively minor compared to the changes in D over the same c range and thus presumably do not exert a substantial influence on the values of D.

Summary

The tracer diffusion of two 3-arm and four 12-arm star PS samples has been investigated as a function of PVME matrix concentration, c, for three different matrix molecular weights, P. The concentration range extended from infinite dilution into the entangled regime. The concentration dependence of the local friction was accounted for approximately using the measured diffusion of the solvent.[1] In addition, the coil contraction of the tracer chains with increasing matrix concentration was determined for one linear, one 3-arm star, and one 12-arm star polymer. The main observations and conclusions may be summarized as follows.

In all cases, D is a smoothly decreasing function of c which is well-described by a stretched exponential form, with fractional exponents generally in the range 0.6–0.75. At fixed M and c, D also decreases with increasing P, indicating that the mobility of the matrix plays a significant role in determining D.

After correction for changing local friction, all the data could be scaled together to form one master curve, when plotted as D/D_0 versus c/c', where c' is a reference concentration selected to give the best superposition. This master curve could also be superposed on the equivalent plot for linear tracer PS, as presented in part 1.[1] However, the values of c' required to achieve the reduction to a master curve were a strong function of f, the number of arms, indicating that while there is evidently considerable universality to the c dependence, the onset of a substantial decrease in D with increasing c occurs at lower c for stars than for linear polymers of equal arm molecular weight. Furthermore, most of the data fall in the transition regime where there are less than five entanglements per molecule,

and thus the apparent universality probably applies more to the transition than to the high-c limit.

The values of D could be compared to those for linear polymers under the same matrix conditions,[1] at constant arm molecular weight, by considering the linear polymers to be 2-arm stars. The ratio D_{star}/D_{linear}, normalized to the infinite dilution values, decreases significantly with increasing c above a concentration that is approximately the entanglement concentration for the matrix, for both 3-arm and 12-arm stars. This is direct evidence that as the solution becomes entangled, a crossover to an architecture-dependent diffusion mechanism occurs. As discussed in the text, currently only the reptation and coupling models are even qualitatively consistent with this observation.

When the same ratio, D_{star}/D_{linear}, is formed at constant total molecular weight, it actually increases slightly with increasing c for the 12-arm stars. This is a result of the fact that the linear polymers become entangled with the matrix at lower concentrations than the rather compact, highly branched stars.

In the highest P solutions, the ratio $D_{3\text{-arm}}/D_{12\text{-arm}}$ at constant arm molecular weight increases with increasing c, as expected, but the corresponding ratio at constant total molecular weight decreases with increasing c. This latter observation also presumably reflects the earlier onset of entanglement for the longer armed molecule. It is not possible on the basis of these comparisons to say whether or not the arm retraction step in the star-reptation picture is quasi-coherent.

The coil contraction of the PS chains with increasing c is significant, but not unusual. The extent of contraction is independent of architecture, as expected (to first order) for a thermodynamically driven process. When plotted against c_{matrix}/c^*_{probe}, the normalized radii of gyration agree very well with the neutron scattering measurements for PS-d in PS solutions, indicating that the slightly negative $\chi_{PS\text{-}PVME}$ has no measurable effect on the coil dimensions in these ternary solutions. This stands as direct support for the assumption underlying much of our work in this area, namely, that PS diffuses through PVME solutions by the same mechanism(s) as through binary PS solutions.

By far the most important result of this study is that star-branched polymers are retarded significantly relative to linear polymers, as the degree of entanglement with the matrix increases. While the diffusion behavior of linear polymers in solution may be reasonably interpreted in several distinct ways, the observation that branched polymers move less rapidly is consistent only with the reptation-based picture.

Acknowledgment. Acknowledgment is made to the donors of the Petroleum Research Fund, administered by the American Chemical Society, for support of this work and to the Graduate School of the University of Minnesota for a Fellowship to L.M.W. We thank Dr. L. J. Fetters for generously providing the branched polymer samples and Dr. H. Watanabe for useful discussions.

Registry No. PS, 9003-53-6; PVME, 9003-09-2.

References and Notes

(1) Wheeler, L. M.; Lodge, T. P. *Macromolecules*, preceding paper in this issue.
(2) de Gennes, P.-G. *J. Chem. Phys.* **1971**, *55*, 572.
(3) de Genes, P.-G. *Scaling Concepts in Polymer Physics*; Cornell University: Ithaca, NY, 1979.
(4) Hess, W. *Macromolecules* **1986**, *19*, 1395.
(5) Hess, W. *Macromolecules* **1987**, *20*, 2587.
(6) Kavassalis, T. A.; Noolandi, J. *Phys. Rev. Lett.* **1987**, *59*, 2674.
(7) Kavassalis, T. A.; Noolandi, J. *Macromolecules* **1988**, *21*, 2869.
(8) Kavassalis, T. A.; Noolandi, J., submitted for publication in *Macromolecules*.
(9) Bueche, F. *J. Chem. Phys.* **1952**, *20*, 1959.
(10) Fujita, H.; Einaga, Y. *Polym. J. (Tokyo)* **1985**, *17*, 1131.
(11) Kolinski, A.; Skolnick, J.; Yaris, R. *J. Chem. Phys.* **1988**, *88*, 1407.
(12) Phillies, G. D. J. *Macromolecules* **1986**, *19*, 2367.
(13) Phillies, G. D. J. *Macromolecules* **1987**, *20*, 558.
(14) Phillies, G. D. J.; Peczak, P. *Macromolecules* **1988**, *21*, 214.
(15) de Gennes, P.-G. *J. Phys. (Les Ulis, Fr.)* **1975**, *36*, 1199.
(16) Klein, J.; Fletcher, D.; Fetters, L. J. *Nature (London)* **1983**, *304*, 526.
(17) Klein, J.; Fletcher, D.; Fetters, L. J. *J. Chem. Soc., Faraday Symp.* **1983**, *18*, 159.
(18) Bartels, C. R.; Crist, B., Jr.; Fetters, L. J.; Graessley, W. W. *Macromolecules* **1986**, *19*, 785.
(19) Antonietti, M.; Sillescu, H. *Macromolecules* **1986**, *19*, 798.
(20) Shull, K. R.; Kramer, E. J.; Hadziiannou, G.; Antonietti, M.; Sillescu, H. *Macromolecules* **1988**, *21*, 2578.
(21) Lodge, T. P.; Wheeler, L. M. *Macromolecules* **1986**, *19*, 2983.
(22) Wheeler, L. M.; Lodge, T. P.; Hanley, B.; Tirrell, M. *Macromolecules* **1987**, *20*, 1120.
(23) Chang, T.-Y.; Han, C. C.; Wheeler, L. M.; Lodge, T. P. *Macromolecules* **1988**, *21*, 1870.
(24) Huber, K.; Burchard, W.; Fetters, L. J. *Macromolecules* **1984**, *17*, 541.
(25) Lodge, T. P.; Markland, P. *Polymer* **1987**, *28*, 1377.
(26) Khasat, N.; Pennisi, R. W.; Hadjichristidis, N.; Fetters, L. J. *Macromolecules* **1988**, *21*, 1100.
(27) Lodge, T. P.; Wheeler, L. M.; Hanley, B.; Tirrell, M. *Polym. Bull. (Berlin)* **1986**, *15*, 35.
(28) Klein, J. *Macromolecules* **1986**, *19*, 105.
(29) Graessley, W. W. *Adv. Polym. Sci.* **1982**, *47*, 67.
(30) Pearson, D. S.; Helfand, E. *Macromolecules* **1984**, *17*, 888.
(31) Rubinstein, M. *Phys. Rev. Lett.* **1986**, *57*, 3023.
(32) Joanny, J. F.; Grant, P.; Pincus, P.; Turkevich, L. A. *J. Phys. (Les Ulis, Fr.)* **1981**, *42*, 1045.
(33) Nose, T. *J. Phys. (Les Ulis, Fr.)* **1986**, *47*, 517.
(34) Daoud, M.; Cotton, J. P.; Farnoux, B.; Jannink, G.; Sarma, G.; Benoit, H.; Duplessix, R.; Picot, C.; de Gennes, P.-G. *Macromolecules* **1975**, *8*, 804.
(35) King, J. S.; Boyer, W.; Wignall, G. D.; Ullman, R. *Macromolecules* **1985**, *18*, 709.
(36) Klotz, S.; Cantow, H.-J.; Kogler, G. *Polym. Bull. (Berlin)* **1985**, *14*, 143.